Circular RNA ZNF827 tunes neuronal differentiation by facilitating transcriptional repression of Neuronal Growth Factor Receptor

Anne Kruse Hollensen[1], Marta Llorett Linares[1], Henriette Sylvain Thomsen[1], Andreas Bjerregaard Kamstrup[1], Jacob Malthe Jensen[2], Majbritt Luckmann[1], Nanna Birkmose[1], Torben Heick Jensen[1], Thomas Birkballe Hansen[1] and Christian Kroun Damgaard[1§]

[1]Department of Molecular Biology and Genetics, Aarhus University, C.F. Møllers Allé 3, Building 1130, DK-8000 Aarhus C, Denmark
[2]Bioinformatics Research Centre, Aarhus University, C.F. Møllers Allé 8, Building 1110, DK-8000 Aarhus C, Denmark Denmark

[§]Corresponding author

Abstract

Circular RNAs (circRNAs) comprise a large class of conserved non-coding RNAs that regulate a number of biological processes, including transcription, alternative splicing, translation and mRNA decay. circRNAs are enriched in the brain and mammalian cells subjected to neuronal differentiation markedly change their circRNA transcriptomes. Here, we have mapped high-confidence circRNA inventories of mouse embryonic stem cells, neuronal progenitor cells and in differentiated glutamatergic neurons and identify hundreds of differentially expressed circRNAs. Among several candidate circRNAs, knockdown of circZNF827 significantly induces expression of key neuronal markers, suggesting that this molecule negatively regulates neuronal differentiation. Using Nanostring analyses we demonstrate that among 770 tested genes linked to known neuronal pathways and neuropathological states, knockdown of circZNF827 deregulates expression of several genes including a robust upregulation of neuronal growth factor receptor (NGFR). We show that NGFR becomes transcriptionally upregulated and that this functionally enhances NGF signalling. Our results suggest that circZNF827, although being highly enriched in the cell cytoplasm, can elicit transcriptional changes, which in turn balances proliferation and neuronal differentiation signalling.

Introduction

The mammalian non-coding transcriptome, which includes long noncoding RNAs (lncRNAs) and circular RNAs (circRNAs), play pivotal roles in biological decisions during differentiation and normal cell maintenance (reviewed in[1-3]). Even though circRNAs were already identified several decades ago[4-7], they have only recently emerged as a large class of abundant noncoding RNAs that exhibit cell type- and tissue-specific expression patterns[8-14] (reviewed in[3,15,16]). CircRNAs are generated by the canonical spliceosome in a non-linear backsplicing fashion[9,10,12,17,18]. During circRNA biogenesis, flanking intronic sequences are thought to bring splice sites within critically close proximity, either by direct basepairing between inverted repeats (e.g. Alu-repeats in primates) or facilitated by interactions between flanking intron-bound RNA-binding proteins (RBPs)[13,15,19]. circRNAs are largely localized to the cell cytoplasm[9-14], and recent evidence suggests that nuclear export of circRNAs in human cells is influenced by the size of the given molecules[20]. Specifically, knockdown experiments have shown that nuclear export of larger circRNAs (>800 nucleotides) are dependent on DExH/D-box helicase UAP56 (DDX39B), whereas smaller species are dependent on URH49 (DDX39A)[20]. At the functional level, several reports have provided evidence that circRNAs play important roles in various fundamental cellular processes. A well described example is the CDR1as/CiRS-7 and SRY circRNAs that function to negatively regulate miR-7 and miR-138 activity, respectively, by sequestration (miRNA sponging), leading to increased mRNA expression of their respective miRNA-targets[11,12]. However, it has been suggested that the majority of circRNAs are likely not *bona fide* miRNA sponges, simply due to relatively low copy numbers and a low number of miRNA binding sites per molecule, leaving efficient miRNA regulation ambigous in many cases[3,15]. Examples of circRNAs acting as binding scaffolds for RBPs, or RBP sponges, which in turn affect their canonical function in e.g. pre-mRNA splicing and protein translation, have been reported[13,21]. Nuclear variants coined exon-intron circular RNAs (EIciRNAs), have, due to their retention of intronic sequences, been shown to promote transcription by recruitment of U1 snRNP to transcription units by a not fully clarified mechanism[22]. Many abundant circRNAs originate from the 5' end of their precursor transcripts, often giving

rise to backsplicing into parts of the 5'UTR of their linear relative[10,12,14], suggesting that at least some circRNAs might have protein-coding potential via a cap-independent translation mechanism, which is consistent with both early studies of Internal Ribosome Entry Sites (IRES) placed in a circRNA context[23], as well as more recent studies reporting examples of translation-compentent circRNAs[24-27]. However, global analyses of hundreds of publicly available ribosome profiling datasets questions the prevalence, frequency and importance of such events[28]. Evidence from RNA-sequencing of RNA isolated from mouse and human tissues along with various cell lines, suggest that circRNAs are most abundantly expressed in the brain, compared to other tissues and that circRNAs are particular enriched in neuronal synaptosomes[14]. In line with this, cells derived from both embryonal carcinoma (P19) and neuroblastoma (SHSY-5Y) subjected to neuronal/glial differentiation show tightly regulated circRNA expression profiles during neuronal development, that include upregulation of numerous common circRNAs[14]. Despite these important advances, evidence to support a causal role of circRNAs in neuronal differentiation and brain development and function are still very limited. Piwecka et al., demonstrated that a circRNA CDR1as knockout mouse displayed downregulated miR-7 levels, alterations in sensorimotor gating associated with neuropsychiatric disease and abnormal synaptic transmission, suggesting that CDR1as and miR-7 is important for normal brain function in the mouse[29]. Adding to the complexity of this regulatory network, a long noncoding RNA (lncRNA), Cyrano, promotes the destruction of miR-7, which in turn upregulates CDR1as by a still unidentified mechanism[30]. Despite this intricate molecular interplay between a circRNA, miRNA and lncRNA, many important questions regarding neuronal differentiation and function remain unanswered. For example, it is currently unknown whether the tightly controlled expression of circRNAs affect neuronal development. Here, we present the circRNA inventory of mouse embryonic stem cells (mESC), neuronal progenitor cells (NPC) and differentiated glutamatergic neurons, which represents a well-established model for CNS-type neuronal differentiation[31]. We report thousands of RNase R-resistant circRNAs of which many are differentially regulated during neuronal development. In a miniscreen for circRNA function using a well-established human model for neuronal differentiation, we identify circZNF827 as a

negative regulator of neuronal differentiation, since multiple neuronal markers (TrkB, NEFL, MAP2, TUBB3, RARs and NGFR) become upregulated upon circZNF827 knockdown, while known negative regulators (PTEN, NQO1 and STAT3) become downregulated. Interestingly, although being almost exclusively localized to the cell cytoplasm, circZNF827 knockdown impact several upregulated genes, including NGFR, at the level of transcription. Taken together, our results suggest that circZNF827 serves to tune the balance between neuronal proliferation and differentiation.

Materials and Methods

Vector construction

To create plasmids for expression of dishRNAs, sense and antisense oligonucleotides (table S1) were annealed and cloned into BglII/XhoI-digested pFRT/U6, resulting in vectors designated pFRT/U6-dishRNA[32]. Subsequently, the U6-dishRNA expression cassettes were PCR-amplified from pFRT/U6-dishRNA vectors (primer sequences are specified in table S1) and inserted into ClaI/BsiWI-digested pCCL/PGK-EGFP-MCS[32]. The resulting lentiviral transfer vectors were designated pCCL/U6-dishRNA-PGK-EGFP-MCS. All plasmids were verified by sequencing.

Cell culturing

L-AN-5 cells were maintained in RPMI and SHSY-5Y and P19 cells were maintained in DMEM medium, both supplemented with 10% fetal calf serum (Gibco) and 1% penicillin/streptomycin (Gibco, 15140122). All cells were cultured at 37°C in 5% (v/v) CO_2. Differentiation of L-AN-5 and SHSY-5Y cells were stimulatied by addition of 10 μM RA to the cell culture medium. Both cell types were differentiated for four days.

mESC culture and differentiation

E14 mESCs were grown on 0.1% gelatin coated plates in 2i medium[33] containing: DMEM/F12 (Gibco, 31331) and Neurobasal (Gibco, 12348) 1:1, N2 supplement (Gibco, 17502048), B27 supplement (Gibco, 17504044), 1X glutaMax (Gibco, 35050061), 1X penicilin/streptomycin (Gibco, 15140122), 1 mM sodyum pyruvate (Gibco, 11360070), 50 nM 2-mercaptoethanol (Gibco, 31350010), nonessential amino acids (Gibco, 11140076), LIF, 3 μM GSK3 inhibitor (CHIR-99021) and 1 μM MEK inhibitor (PD0325901). They were differentiated into neurons as previously described[31] with some modifications. 4 million cells were differentiated into embryoid bodies in suspension in petri dishes for bacterial culture in 15ml medium containing the same as before, but with 10% FBS and without LIF or GSK3 and MEK inhibitors. Every second day, the medium was changed and the embryoid bodies transferred to fresh petri dishes. On days 4 and 6, 5 μM ATRA (sigma, R2625) was added to the medium. On day 8 of differentiation, the embryoid bodies were disgregated

with 5% trypsin (Gibco, 15400054) and the cells plated in poly-DL-ornithine (Sigma, P8638) and laminin (Sigma, L2020) coated plates in N2 medium, containing DMEM/F12 and neurobasal 1:1, N2 supplement, sodium pyruvate, glutaMax, 15 nM 2-mercaptoethanol, and 50 µg/ml BSA. The medium was changed after 2 h and after 24 h. 48 h after plating the neuronal precursors, the medium was changed to complete medium, containing B27 supplement, in addition to the N2 medium. Neurons were harvested 2 and 8 days after plating.

Lentiviral production

Third-generation lentiviral vectors were produced in HEK293T cells as previously described[34]. One day before transfection, cells were seeded in 10-cm dishes at a density of 4×10^6 cells/dish. Transfections were carried out with 3.75 µg pMD.2G, 3 µg pRSV-Rev, 13 µg pMDLg/pRRE and 13 µg lentiviral transfer vector using a standard calcium phosphate or polyethylenimine transfection protocol. Medium was changed to RPMI medium one day after transfection. Two days after transfection viral supernatants were harvested and filtered through 0.45 µm filters (Sartorius). All lentiviral preparations were made in at least triplicates and pooled before determination of viral titers. To determine viral titers of lentiviral preparations, flow cytometric measurements of EGFP expression were used as previously described[34]. One day prior to transduction, L-AN-5 cells were seeded at a density of 5×10^5 cells/well in 12-well plates. For all lentiviral preparations, transductions with 10^2- and 10^3-fold dilutions of virus-containing supernatants were carried out. Both viral supernatants and growth medium were supplemented with 4 µg/ml polybrene (Sigma-Aldrich). One day after transduction, medium was changed. Five days after transduction, cells were harvested and fixated in 4% paraformaldehyde (Sigma-Aldrich). EGFP expression levels were analyzed on a CytoFLEX flow cytometer (Beckman Coulter). Lentiviral titers were calculated based on samples with between 1% and 20% EGFP positive cells using the formula: titer (TU/ml) = $F \cdot C_n \cdot DF/V$, where F represents the frequency of EGFP positive cells, C_n the total number of target cells counted the day the transductions were carried out, DF the dilution factor of the virus and V the volume of transducing inoculum.

circRNA knockdown and differentiation

One day prior to transduction with lentiviral vectors encoding circRNA-specific dishRNAs, L-AN-5 cells were seeded at a density of 2.2 x 10^6 cells/dish in 6-cm dishes or 0.8 x 10^6 cells/well in 6-well plates. Transductions were carried out using equal MOIs calculated based on titers determined by flow cytometry. Both viral supernatants and growth medium were supplemented with 4 μg/ml polybrene. One day after transduction, medium was changed. Two days after transduction, differentiation was initiation by addition of 10 μM RA to the cell culture medium. The L-AN-5 and SHSY-5Y cells were differentiated for four days.

BrU pulse-chase mRNA decay assay

Lentiviral transduction and RA-mediated differentiation of L-AN-5 cells were carried out as described in the section 'circRNA knockdown and differentiation'. The L-AN-5 cells were cultured in 6-cm dishes containing 6 ml cell culture medium supplemented with 10 μM RA. 4 ml cell culture medium was aspirated from each 6-cm dish and pooled from cells transduced with the same dishRNA. For one dish per dishRNA, the residual medium was aspirated and 3.5 ml of the collected medium was added. For the remaining dishes, the residual medium was aspirated and 3.5 ml of the collected medium supplemented with 2 mM BrU (Thermo-Fisher) was added. 1 hour after addition of BrU to the cell culture medium, the cells were washed three times in cell culture medium. 50 min after removal of the BrU-containing cell culture medium the first samples including the samples not treated with BrU were harvested. Subsequently, samples were harvested after 3, 6 and 9 hours. Total RNA was purified using 1 ml TRI Reagent (Sigma-Aldrich) according to manufacturer's protocol. circRNA knockdown and differentiation of L-AN-5 cells were verified by RT-qPCR using total RNA as described in the section 'Quantitative PCR'. BrU-labeled RNA was immunoprecipitated as described elsewhere[35]. Briefly, BrdU antibodies were conjugated to magnetic beads. 15 µl Dynabeads M-280 Sheep Anti-Mouse IgG (Invitrogen) per sample were washed twice in 1x BrU-IP buffer (20 mM Tris-HCl (pH 7.5), 250 mM NaCl, 0.5 µg/µl BSA, 20 U/ml RiboLock (Thermo-Fisher) and

resuspended in 1 ml 1x BrU-IP buffer with heparin (20 mM Tris-HCl (pH 7.5), 250 mM NaCl, 1 mg/ml heparin). After 30 min of incubation at room temperature on a rotator the beads were washed in 1x BrU-IP buffer. Subsequently, the beads were resuspended in 1 ml 1x BrU-IP buffer supplemented with 0.9 µl mouse BrdU antibody (BD Pharmingen, clone 3D4) per sample and incubated for 1 hour at room temperature on a rotator. The beads were washed three times in 1x BrU-IP buffer and resuspended in 50 µl 1x BrU-IP buffer supplemented with 1 mM 5-BrU per sample. After 30 min of incubation at room temperature on a rotator the beads were washed three times in 1x BrU-IP buffer and resuspended in 50 µl 1x BrU-IP buffer per sample. 25 µg of total RNA was diluted to 200 µl and incubated at 80°C for 2 min. 200 µl 2x BrU-IP buffer with BSA and RiboLock (20 mM Tris-HCl (pH 7.5), 250 mM NaCl, 1 µg/µl BSA, 80 U/ml RiboLock (Thermo-Fisher) and 50 µl beads conjugated with BrdU antibodies were added to the RNA samples. After 1 hour of incubation at room temperature on a rotator the beads were washed once in four times in 1x BrU-IP buffer. For elution of immunoprecipitated RNA the beads were resuspended in 200 µl 0.1% SDS. RNA was purified by phenol/chloroform extraction, ethanol precipitation and the RNA pellets were resuspended in 10 µl nuclease free water. 2 µl of immunoprecipitated RNA was used for quantification of mRNA expression levels by RT-qPCR as described in the section 'Quantitative PCR' except that DNase treatment was omitted and 1 µg yeast RNA (Roche) was added in the cDNA reaction.

BrU-labeling and immunoprecipitation of newly synthesized RNA

The BrU-labeling and immunoprecipitation of newly labeled RNA were carried out as for the mRNA decay assay except that the cells were harvested 45 min after addition of BrU to the cell culture medium. Furthermore, after binding of the RNA to the beads, the beads were washed once in 1x BrU-IP buffer, twice in 1x BrU-IP buffer supplemented with 0.01% Triton X-100 and twice in 1x BrU-IP buffer.

Subcellular fractionation of nuclear and cytoplasmic RNA

Subcellular fractionation of nuclear and cytoplasmic RNA was carried out as previously described in[36]. Briefly, cells were washed in PBS, added 800 µl

PBS and scraped off. 100 µl of the cell solution was centrifuged at 12,000 rpm for 10 sec at 4°C. Cell pellets were used for purification of total RNA using 1 ml of TRI Reagent (xx) according to manufacturer's protocol. The remaining 700 µl of the cell solution was used for subcellular fractionation of nuclear and cytoplasmic RNA. After centrifugation at 12,000 rpm for 10 sec at 4°C cell pellets were added 300 µl lysis buffer (20 mM Tris-HCl (pH 7.5), 140 mM NaCl, 1 mM EDTA, 0.5% Igepal-630 (Nonidet P-40)), incubated on ice for 2 min and centrifugated at 1000 g for 4 min at 4°C. Cytoplasmic RNA was purified from the supernatants using 1 ml TRI Reagent (Sigma-Aldrich) according to manufacturer's protocol. Pellets were washed twice in 500 µl lysis buffer, subjected to a single 5 sec pulse of sonication at the lowest settings (Branson Sonifier 250) and nuclear RNA was purified using 1 ml TRI Reagent (Sigma-Aldrich) according to manufacturer's protocol.

NGF stimulation

Lentiviral transduction and RA-mediated differentiation of L-AN-5 cells were carried out as described in the section 'circRNA knockdown and differentiation'. After four days of differentiation the cells were stimulated with 200 ng/ml NGF (Life Technologies) for 30 min and subsequently harvested in TRI reagent (Thermo Fisher Scientific) for RNA purification.

Quantitative PCR

RNA was purified using TRI reagent (Thermo Fisher Scientific) according to manufacturer's protocol. RNA samples were treated with DNase I (Thermo Fisher Scientific) according to manufacturer's protocol. First-strand cDNA synthesis was carried out using the Maxima First Strand cDNA synthesis Kit for qPCR (Thermo Fisher Scientific) according to manufacturer's protocol. qPCR reactions were prepared using gene-specific primers (table S1) and Platinum SYBR Green qPCR Supermix-UDG (Thermo Fisher Scientific) according to manufacturer's protocol. An AriaMx Real-time PCR System (Agilent Technologies) was used for quantification of RNA levels and the X_0 method was used for calculations of relative RNA levels (Thomsen et al., 2010, J Bioinform Comput Biol) normalized to either GAPDH or beta-actin mRNA as indicated.

NanoString

Gene expression analysis of 770 neuropathology-related genes were analyzed using the nCounter Human Neuropathology Panel (NanoString Technologies) and the nCounter *SPRINT* Profiler (NanoString Technologies) according to manufacturer's protocol. Data analysis was carried out in the nSolver 4.0 software (NanoString Technologies) using the nCounter Advanced Analysis Software (NanoString Technologies).

Cell proliferation assay

Lentiviral transduction and RA-mediated differentiation of L-AN-5 cells were carried out as described in the section 'circRNA knockdown and differentiation'. Labeling of newly synthesized DNA was carried out using Click-iT Plus EdU Alexa Flour 647 Flow Cytometry Assay Kit (Thermo Fisher Scientific) according to manufacturer's protocol. Notably, the cell culture medium of L-AN-5 cells cultured in 6-well plates was supplemented with 10 µM EdU for 1.5 hours. To stain total DNA, cells with already detected EdU were resuspended in 400 µl 1x Click-iT saponin-based permeabilization and wash reagent from the Click-iT Plus EdU Alexa Flour 647 Flow Cytometry Assay Kit (Thermo Fisher Scientific). Subsequently, RNase A was added to af final concentration of 0.2 mg/ml. After 5 min of incubation at room temperature, propidium iodide was added to af final concentration of 5 µg/ml and the cells were incubated for 30 min at room temperature. Incorporated EdU and total DNA levels were analyzed on a BD LSRFortessa flow cytometer (BD Biosciences). Data analysis was carried out in the FLOWJO software (BD Biosciences).

Western blotting

Cells were scraped off, pelleted and lysed for 15 min on ice in RSB100 (10 mM Tris-HCl (pH 7.4), 100 mM NaCl, 2.5 mM $MgCl_2$) supplemented with 0.5% Triton X-100 and 1 cOmplete, Mini, EDTA-free, protease inhibitor cocktail tablet (Roche).

The cell lysates were subjected to two 5 sec pulses of sonication at the lowest settings (Branson Sonifier 250) followed by centrifugation at 4000 g for 15 min at 4°C. Glycerol were added to the supernatnats (final concentration: 10%) and protein concentrations were adjusted using Bradford protein assay dye

(Bio-Rad). The protein samples were diluted in 6x loading buffer (), heated at 95°C for 3 min and seprated on a Novex WedgeWell 4-12% Tris-Glycine Gel (Invitrogen). Proteins were transferred to an PVDF Transfer Membrane (Thermo Scientific) using standard procedures. The membrans were blocked in 5% skimmed milk powder in PBS for 1 hour at room temperature. The membranes were incubated at 4°C overnight with primary antibodies diluted as indicated in table Sx in 5% skimmed milk powder in PBS. After three times wash, the membranes were incubated with goat polyclonal HRP-conjungated secondary antibodies (Dako) diluted 1:20000 in 5% skimmed milk powder in PBS. After 1 hour of incubation at room temperature, the membranes were washed three times and the bound antibodies were detected using the SuperSignal West Femto maximum sensitivity substrate (Thermo Scientific) according to manufacturer's protocol and the LI-COR Odyssey system (LI-COR Biosciences).

Statistical Analysis

In biochemical assays (conducted in at least biological triplicates) the significance of difference between samples were calculated by a two-tailed Student's t test to test the null hypothesis of no difference between the two compared groups. The assumption of equal variances was tested by an F test. $p < 0.05$ was considered statistically significant. Data are presented as mean ± SD. The DEseq2 pipeline[37], which is based on the negative binomial distribution and estimates the variance-mean dependence in count data from high-throughput sequencing experiments was used to test for differential expression. pAdj <0.05 from biological triplicates were taken as significant differences.

Results

The circRNA profile of mESC changes markedly upon neuronal differentiation.

To determine whether circRNAs influence neuronal differentiation, we initially sought to confidently map the circRNA inventories at different stages of neuronal differentiation and compare this to other available circRNA datasets of neuronal origin from mice and humans[14]. Identification of circRNAs from RNA-seq experiments has often been based on quantification of relatively few

reads across the unique circRNA backsplicing junction (circBase[38]), and current circRNA prediction algorithms inevitably lead to the calling of false positives[39,40]. Hence, to immediately validate the circular nature of *to-be* called circRNAs, we first performed standard rRNA depletion and subsequently either included or excluded an RNase R treatment step prior to RNA-sequencing. Specifically, we used an established differentiation model for CNS-type glutamatergic neurons, based on E14 mouse embryonic stem cells (mESCs) that reportedly yields a purity of glutamatergic neurons of >90%[31]. RNA was isolated from 3 stages of differentiation, mESCs, neuronal progenitor cells (NPCs) or neuronal differentiation day 8 (N8) and rRNA depleted (+/- RNase R) prior to library preparation and RNA-seq (Illumina platform) (Figure 1A). Successful differentiation at the NPC and N8 stages was confirmed by the appearance of elongated inter-cellular dendritic extensions (N8) (Figure S1A) and robust upregulation of several classical neuronal markers including, nTrk, MAP2 and TUBB3 (NPC and N8), while stem cell pluripotency markers, including Nanog became significantly reduced upon differentiation (Figure S1B). Using available circRNA prediction tools CIRI2[41], find_circ[12] and CIRCexplorer2[42] first on the non-RNase R-treated RNA, we identified between 792-1167 circRNAs in mESC, 2230-2893 circRNAs in NPC and 1902-2316 circRNAs in differentiated neurons (Figure 1B). Upon treatment of the RNA samples with RNase R most circRNAs either remained unchanged or became enriched, but a considerable fraction of the predicted circRNAs in mESC, NPC and N8 preparations, became depleted by the exonuclease (CIRCexplorer2: 19.5-36.5%; CIRI2: 7.2-16.6%; find_circ: 38.7-52.3% depleted) (Figure S1C). All prediction algorithms revealed a relatively strong bias for depletion of low expressed circRNAs (Figure S1D). From a total of 3581 unchanged or enriched circRNAs after RNase R treatment (all stages), 1449 circRNAs overlapped between all 3 circRNA prediction algorithms, and this subset represents a high-confidence circRNA inventory[39] (Figure 1C and Table S2). We next assessed the *circular-to-linear* ratio of identified circRNAs (find_circ), by comparing splice site usage in circular vs. linear splicing events. This analysis revealed vast differences in the steady-state levels of these isoforms and demonstrated that many circRNA species are considerably more abundant than their linear precursors (Figure 1D). Confirming previous studies, the introns flanking the circRNAs

are generally longer than average introns and circRNAs often tend to cluster at the 5' end of their respective precursor RNA, yielding an enrichment in canonical 5'UTRs of the precursor RNAs (Figure S1E-F). Our results suggest that in order to obtain high confidence circRNA inventories from RNA-seq data, it is important to use multiple circRNA prediction algorithms and further beneficial to enrich for bona fide circRNAs, by depletion of linear RNAs using RNase R.

We next assessed differential circRNA expression during differentiation, which revealed marked changes in circRNA expression over the 14-day timecourse. Statistical analyses demonstrated differential expression of 116 circRNAs advancing from mESC to the neuronal stage (>2 log2FC; DESeq2 p-value<0.05, pAdj<0.136) (Figure 1E; left panel and Table S3), clustering in 5 different expression patterns (k-means analysis, Figure 1E; top panel). Comparison with previously identified mouse and human homologue circRNAs isolated from mouse brain regions or cell lines of either murine or human origin[14], revealed significant overlap between circRNAs at differentiated stages (e.g. 80% to differentiated murine p19 cells 45% to human SH-SY5Y and 75% overlap with circRNAs found in the human ENCODE data). We confirmed differential expression of a subset of the most abundant and upregulated circRNAs (circTulp4, circMagi1, circRmst, circEzh2, circHdgfrp3, circZfp827, circMed13L, circZfp609, circSlc8a1, circNfix, circAff3, circAnkib1) using RT-qPCR with amplicons across the backsplicing junction (Figure 1F-G). 75% of the top-100 expressed mouse circRNAs was also found in human circRNA datasets[14]. We conclude that significant changes in circRNA expression patterns are induced upon neuronal differentiation and that the majority of these circRNAs are conserved between various neuronal cell-types originating from humans and the mouse.

Knockdown of circZNF827 stimulates neuronal marker expression

To ascertain whether highly upregulated circRNAs might contribute to the process of neuronal differentiation themselves, we next depleted a number of candidate circRNAs by RNAi. Since mESCs are notoriously hard to transfect, we first tested knockdown efficiency of circZfp827 (circZNF827 in humans) by lentivirally delivered dishRNAs[32] targeting the backsplicing junction in either mESC, p19, SH-SY5Y or L-AN-5 cells, of which the latter three cell lines are

well established models of neuronal differentiation following retinoic acid treatment. Knockdown efficiency in mESC and p19 proved relatively poor (30-60% remaining circRNA) compared to the two human cell lines, SH-SY5Y (10% remaining) of which L-AN-5 displayed superior results (<8% remaining) (Figure S2A and Figure 2A). Moreover, when testing the increase of neuronal differentiation markers TrkB, NEFL, MAP2 and TUBB3 upon retinoic acid treatment, L-AN-5 elicited a more dynamic expression pattern compared to SH-SY5Y cells where only TrkB was upregulated upon differentiation (Figure S2B and Figure 2B). We therefore tested knockdown of 14 candidate circRNAs (circTULP4, circSLC8A1, circZNF609, circHDGFRP3, circZNF827, circANKIb, circCDYL, circUNC79, circCAMSAP1, circMAGI1, circRMST, circMED13L, circHIPK3, circNFIX) (Figure S2C) in L-AN-5 cells and subsequently subjected these to retinoic acid-induced differentiation, followed by neuronal marker quantification to probe for changes in differentiation. Only knockdown of circZNF827 produced a significant increase in neuronal marker expression upon differentiation (Figure 2B-C). Importantly, the linear ZNF827 mRNAs were not affected by backsplicing junction-specific knockdown (Figure S2E). The upregulation of neuronal markers following circZNF827 knockdown, were also evident at the protein level for MAP2 and TUBB3 (Figure 2C). In addition, proliferation assays demonstrated only a marginally smaller S-phase population (lowered from 31% to 23%) upon circZNF827 knockdown, suggesting slightly lowered replication kinetics (Figure 2D). This phenomenon was accompanied by a slight stall in G_2/M phase, while G_2/G_1 phase was not significantly affected between control and circZNF827 knockdown. Taken together, our results suggest that circZNF827 exert a repressive effect on neuronal differentiation.

circZNF827 controls retinoic acid receptor homeostasis

We next asked whether the Retinoic Acid Receptors (RARs), which represent central nodes in relaying anti-proliferative differentiation cues during neuronal development[43], and are key targets of retinoic acid, also become upregulated upon knockdown of circZNF827. Indeed, knockdown of circZNF827 leads to a moderate but significant increased expression (1.5-2.5 fold) of RARα and RARγ (Figure 3A). Since most circRNAs have been reported to predominantly

localize in the cell cytoplasm, we addressed the localization of circZNF827, circTULP4 and circANKIb by cellular fractionation. All three circRNAs are mainly cytoplasmically localized in L-AN-5 cells (~90% cytoplasmic signal) (Figure 3B). We therefore speculated that circZNF827 could potentially affect RAR-mRNA stability post-transcriptionally in the cell cytoplasm. However, BrU pulse-chase mRNA decay assays demonstrated no significant change in RAR-mRNA decay rates upon knockdown of circZNF827 (Figure 3C). Next, we investigated transcription rates, by treating cells with a short pulse of BrU, followed by BrU immunoprecipitation to quantify *de novo* labeled RNA, which serves as a proxy for transcription rates during control- or knockdown of circZNF827. As expected from the constant mRNA decay rates, transcription was slightly, but significantly, upregulated upon circZNF827 knockdown (Figure S3A). Our results suggest that circZNF827 may contribute to fine-tuning of RA-receptor transcription, which in turn will likely keep neuronal differentiation in check.

circZNF827 knockdown affect multiple genes in neuronal signaling

Our results indicate that L-AN-5 cells slow their proliferation and promote RAR-signalling by a slight transcriptional upregulation of these receptor transcription factors when circZNF827 levels are low. To address more global effects of circZNF827 knockdown, we performed NanoString analyses using a neuro-differentiation/pathology panel of ~800 genes on RNA purified from differentiated or non-differentiated cells. Numerous genes become differentially expressed due to circZNF827 knockdown after differentiation (Figure 4A, Table S3). In line with a potential negative regulatory function of circZNF827 on neuronal differentiation, GO-term analyses show enrichment of terms including axon/dendrite structure, neural cytoskeleton, transmitter synthesis, neural connectivity, growth factor signaling and trophic factors among upregulated genes, during circZNF827 knockdown (Figure 4B).

Among the most significantly upregulated genes is Neuronal Growth Factor Receptor (NGFR), which plays a central role in regulating neuronal differentiation, death, survival and neurite outgrowth[44,45]. Furthermore, Phosphatase and tensin homolog (PTEN), STAT3 and NAD(P)H quinone dehydrogenase 1 (NQO1) were all significantly downregulated upon circZNF827 knockdown (2-4 fold), consistent with reported positive roles of

these factors in neuronal differentiation[46,47] and the induction susceptibility to energetic and proteotoxic stress[48]. We next validated the NGFR upregulation, using both qRT-PCR and western blotting, which demonstrated a massive upregulation at both the protein and mRNA level (Figure 4C and S4A). This upregulation was not due to changes in mRNA decay rates, since BrU pulse-chase mRNA decay assays yielded very similar mRNA half-lives upon circZNF827 knockdown (Figure 4D). To address whether the observed changes in gene expression is elicited at the transcriptional or post-transcriptional level, we subjected cells to a short BrU-pulse prior to BrU immunoprecipitation and NanoString hybridization. Interestingly, NGFR and also ATP8A2 proved to be highly upregulated (~4-6 fold) at the level of transcription (Figure 4E-F), while only NQO1 and not PTEN and STAT3 exhibited significantly reduced transcription activity (ranging from ~1.3 to ~4 fold) (Figure 4E). Also, the MAP2 gene did not change its *de novo* RNA output, suggesting that the tuning of the steady-state levels of PTEN, STAT3 and MAP2 mRNAs, initially observed are mainly facilitated by post-transcriptional changes to mRNA stability.

Finally, we sought to functionally validate the impact of NGFR upregulation upon circZNF827 knockdown. To this end, we NGF-treated L-AN-5 cells subjected to either control or circZNF827 knockdown, and quantified downstream signaling output by quantification of c-fos, which is a well-known downstream immediate early target of NGFR signaling. c-fos levels increased significantly, strongly indicating that the higher levels of NGFR protein indeed leads to functional increase in NGFR signaling (Figure 4G), which can at least in part explain the upregulation of classical neuronal markers. Taken together, we conclude that circZNF827 serves to keep neuronal differentiation 'in check' by limiting both RARs and to a larger extent NGFR.

Discussion

Circular RNAs are by now considered as an important class of abundant and conserved RNAs and their functional potential has likely not been fully elucidated. Here, we have identified high-confidence circRNA inventories of E14 mESCs, NPCs and differentiated glutamatergic neurons and generally show a high degree of conservation among circRNAs previously identified using cell lines and tissues of neuronal origin[14]. The 3 different circRNA

prediction pipelines, CIRI2[41], find_circ[12] and CIRCexplorer2[42], displayed marked differences in their predictions, which is in line with our earlier observations[39]. This could indicate that many reported circRNAs are likely false positives, especially when expressed at low levels. A surprisingly large fraction of initially called circRNAs become depleted upon RNase R treatment (between 7,2% and 52,3%), with CIRI2 clearly being the most robustly performing predictor in terms of RNase R resistance. Among 3581 RNase R-resistant circRNAs, only 1449 were called by all three algorithms, suggesting that caution should be taken when predicting circRNAs from RNA-seq data and that including multiple prediction algorithms and/or an RNase R step prior to RNA-seq is beneficial.

Analyzing circRNA expression over the 3 neuronal developmental stages, we identified 116 differentially expressed circRNAs (>2-fold change) and knockdown of circZNF827 in human L-AN-5 cells had a significant and positive impact on the expression of several classical neuronal markers, suggesting that the circRNA normally exerts a negative role in neuronal differentiation. Among nearly 800 genes, important to neuronal differentiation and disease, we found that NGFR ($p75^{NTR}$) was most strongly induced, also at the protein level, upon circZNF827 knockdown. NGFR is a member of the TNF superfamily of receptors and relays, along with 3 paralogous receptor tyrosine kinases (TrkA, TrkB and TrkC), signals from the 4 mammalian neurotrophins (Nerve Growth Factor (NGF), brain-derived neurotrophic factor (BDNF), neurotrophin-3 (NT-3) and neurotrophin 4 (NT-4, aka. NT-4/5)[45]. The regulation and functional output from the neurotrophins and their receptors, which are interdependent proteins, is extremely complex and involves a multitude of effector proteins and interaction partners[45]. NGFR can, depending on expression levels of also the other neurotrophin receptors and their ligands, either induce death- or survival signaling to promote neuronal differentiation and control axonal growth or apoptosis[45]. Whether NGFR upregulation is instrumental and causal for the enhanced expression of TrkB, NEFL, TUBB3 and MAP2 that we observe in the L-AN-5 neuroblastoma system, remains to be seen. However, we did observe strongly augmented c-fos expression (immediate early gene) upon treatment of L-AN-5 cells with NGF, when circZNF827 was downregulated, which may suggest that TrkA-mediated NGF response becomes enhanced by increased NGFR expression.

How does circZNF827 regulate transcription rates of the NGFR gene and does this regulation involve a direct effect? Since circZNF827 is largely cytoplasmic (90%) it is tempting to speculate that positive transcription regulators (i.e. chromatin remodeling factors) with RNA-binding capacity, may become sequestered in this compartment by the circRNA. Supporting such a model is the finding that many classical DNA-binding transcription factors and co-regulators also interact with RNA[49-51]. That circRNAs can sequester effectors is reminiscent of the reported sequestration of splicing regulator MBL by a circRNA generated from its own pre-mRNA[13]. Alternatively, the nuclear fraction of the circZNF827 population could potentially regulate transcription in a fashion similar to that of long non-coding RNAs (lncRNAs). Transcriptional regulation has already been reported for intron-containing circRNAs ElciRNAs[22], but not for the regular circRNAs. While we have demonstrated circRNA-mediated transcriptional regulation of NGFR in differentiating neurons, further studies are required to determine the mechanism of action and to disclose whether or not the process involves a direct intersection with DNA/RNA-binding regulators of transcription in the cytoplasm and/or the nucleus.

Acknowledgement

We thank Karina Hjorth for excellent technical assistance. We are thankful to Novo Nordisk Foundation for support for this research (NNF13OC0007719 and NNF17OC0028804). Proliferation assays using flow cytometry was performed at the FACS Core Facility, Aarhus University, Denmark.

References

1 Deveson, I. W., Hardwick, S. A., Mercer, T. R. & Mattick, J. S. The Dimensions, Dynamics, and Relevance of the Mammalian Noncoding Transcriptome. *Trends Genet* **33**, 464-478, doi:10.1016/j.tig.2017.04.004 (2017).

2 Kopp, F. & Mendell, J. T. Functional Classification and Experimental Dissection of Long Noncoding RNAs. *Cell* **172**, 393-407, doi:10.1016/j.cell.2018.01.011 (2018).

3 Chekulaeva, M. & Rajewsky, N. Roles of Long Noncoding RNAs and Circular RNAs in Translation. *Cold Spring Harb Perspect Biol*, doi:10.1101/cshperspect.a032680 (2018).

4 Nigro, J. M. *et al.* Scrambled exons. *Cell* **64**, 607-613 (1991).

5 Capel, B. *et al.* Circular transcripts of the testis-determining gene Sry in adult mouse testis. *Cell* **73**, 1019-1030 (1993).

6 Kos, A., Dijkema, R., Arnberg, A. C., van der Meide, P. H. & Schellekens, H. The hepatitis delta (delta) virus possesses a circular RNA. *Nature* **323**, 558-560, doi:10.1038/323558a0 (1986).

7 Sanger, H. L., Klotz, G., Riesner, D., Gross, H. J. & Kleinschmidt, A. K. Viroids are single-stranded covalently closed circular RNA molecules existing as highly base-paired rod-like structures. *Proceedings of the National Academy of Sciences of the United States of America* **73**, 3852-3856 (1976).

8 Salzman, J., Chen, R. E., Olsen, M. N., Wang, P. L. & Brown, P. O. Cell-type specific features of circular RNA expression. *PLoS Genet* **9**, e1003777, doi:10.1371/journal.pgen.1003777 (2013).

9 Salzman, J., Gawad, C., Wang, P. L., Lacayo, N. & Brown, P. O. Circular RNAs are the predominant transcript isoform from hundreds of human genes in diverse cell types. *PloS one* **7**, e30733, doi:10.1371/journal.pone.0030733 (2012).

10 Jeck, W. R. *et al.* Circular RNAs are abundant, conserved, and associated with ALU repeats. *RNA* **19**, 141-157, doi:10.1261/rna.035667.112 (2013).

11 Hansen, T. B. *et al.* Natural RNA circles function as efficient microRNA sponges. *Nature* **495**, 384-388, doi:10.1038/nature11993 (2013).

12 Memczak, S. *et al.* Circular RNAs are a large class of animal RNAs with regulatory potency. *Nature* **495**, 333-338, doi:10.1038/nature11928 (2013).

13 Ashwal-Fluss, R. *et al.* circRNA biogenesis competes with pre-mRNA splicing. *Mol Cell* **56**, 55-66, doi:10.1016/j.molcel.2014.08.019 (2014).

14 Rybak-Wolf, A. *et al.* Circular RNAs in the Mammalian Brain Are Highly Abundant, Conserved, and Dynamically Expressed. *Mol Cell* **58**, 870-885, doi:10.1016/j.molcel.2015.03.027 (2015).

15 Ebbesen, K. K., Hansen, T. B. & Kjems, J. Insights into circular RNA biology. *RNA biology*, 1-11, doi:10.1080/15476286.2016.1271524 (2016).

16 Salzman, J. Circular RNA Expression: Its Potential Regulation and Function. *Trends Genet* **32**, 309-316, doi:10.1016/j.tig.2016.03.002 (2016).

17 Cocquerelle, C., Mascrez, B., Hetuin, D. & Bailleul, B. Mis-splicing yields circular RNA molecules. *FASEB J* **7**, 155-160 (1993).

18 Pasman, Z., Been, M. D. & Garcia-Blanco, M. A. Exon circularization in mammalian nuclear extracts. *RNA* **2**, 603-610 (1996).

19 Conn, S. J. *et al.* The RNA binding protein quaking regulates formation of circRNAs. *Cell* **160**, 1125-1134, doi:10.1016/j.cell.2015.02.014 (2015).

20 Huang, C., Liang, D., Tatomer, D. C. & Wilusz, J. E. A length-dependent evolutionarily conserved pathway controls nuclear export of circular RNAs. *Genes Dev* **32**, 639-644, doi:10.1101/gad.314856.118 (2018).

21 Abdelmohsen, K. *et al.* Identification of HuR target circular RNAs uncovers suppression of PABPN1 translation by CircPABPN1. *RNA biology* **14**, 361-369, doi:10.1080/15476286.2017.1279788 (2017).

22 Li, Z. *et al.* Exon-intron circular RNAs regulate transcription in the nucleus. *Nature structural & molecular biology* **22**, 256-264, doi:10.1038/nsmb.2959 (2015).

23 Chen, C. Y. & Sarnow, P. Initiation of protein synthesis by the eukaryotic translational apparatus on circular RNAs. *Science* **268**, 415-417 (1995).

24 AbouHaidar, M. G., Venkataraman, S., Golshani, A., Liu, B. & Ahmad, T. Novel coding, translation, and gene expression of a replicating covalently closed circular RNA of 220

nt. *Proceedings of the National Academy of Sciences of the United States of America* **111**, 14542-14547, doi:10.1073/pnas.1402814111 (2014).
25 Legnini, I. *et al.* Circ-ZNF609 Is a Circular RNA that Can Be Translated and Functions in Myogenesis. *Mol Cell* **66**, 22-37 e29, doi:10.1016/j.molcel.2017.02.017 (2017).
26 Pamudurti, N. R. *et al.* Translation of CircRNAs. *Mol Cell* **66**, 9-21 e27, doi:10.1016/j.molcel.2017.02.021 (2017).
27 Yang, Y. *et al.* Extensive translation of circular RNAs driven by N(6)-methyladenosine. *Cell Res* **27**, 626-641, doi:10.1038/cr.2017.31 (2017).
28 Stagsted, L. V., Nielsen, K. M., Daugaard, I. & Hansen, T. B. Noncoding AUG circRNAs constitute an abundant and conserved subclass of circles. *Life Sci Alliance* **2**, doi:10.26508/lsa.201900398 (2019).
29 Piwecka, M. *et al.* Loss of a mammalian circular RNA locus causes miRNA deregulation and affects brain function. *Science*, doi:10.1126/science.aam8526 (2017).
30 Kleaveland, B., Shi, C. Y., Stefano, J. & Bartel, D. P. A Network of Noncoding Regulatory RNAs Acts in the Mammalian Brain. *Cell* **174**, 350-362 e317, doi:10.1016/j.cell.2018.05.022 (2018).
31 Bibel, M., Richter, J., Lacroix, E. & Barde, Y. A. Generation of a defined and uniform population of CNS progenitors and neurons from mouse embryonic stem cells. *Nat Protoc* **2**, 1034-1043, doi:10.1038/nprot.2007.147 (2007).
32 Kaadt, E. *et al.* Efficient Knockdown and Lack of Passenger Strand Activity by Dicer-Independent shRNAs Expressed from Pol II-Driven MicroRNA Scaffolds. *Mol Ther Nucleic Acids* **14**, 318-328, doi:10.1016/j.omtn.2018.11.013 (2019).
33 Ying, Q. L. *et al.* The ground state of embryonic stem cell self-renewal. *Nature* **453**, 519-523, doi:10.1038/nature06968 (2008).
34 Hollensen, A. K. *et al.* Improved microRNA suppression by WPRE-linked Tough Decoy microRNA sponges. *RNA*, doi:10.1261/rna.061192.117 (2017).
35 Meola, N. *et al.* Identification of a Nuclear Exosome Decay Pathway for Processed Transcripts. *Mol Cell* **64**, 520-533, doi:10.1016/j.molcel.2016.09.025 (2016).
36 Hollensen, A. K. *et al.* Improved microRNA suppression by WPRE-linked tough decoy microRNA sponges. *RNA* **23**, 1247-1258, doi:10.1261/rna.061192.117 (2017).
37 Love, M. I., Huber, W. & Anders, S. Moderated estimation of fold change and dispersion for RNA-seq data with DESeq2. *Genome biology* **15**, 550, doi:10.1186/s13059-014-0550-8 (2014).
38 Glazar, P., Papavasileiou, P. & Rajewsky, N. circBase: a database for circular RNAs. *RNA* **20**, 1666-1670, doi:10.1261/rna.043687.113 (2014).
39 Hansen, T. B., Veno, M. T., Damgaard, C. K. & Kjems, J. Comparison of circular RNA prediction tools. *Nucleic acids research*, doi:10.1093/nar/gkv1458 (2015).
40 Jeck, W. R. & Sharpless, N. E. Detecting and characterizing circular RNAs. *Nat Biotechnol* **32**, 453-461, doi:10.1038/nbt.2890 (2014).
41 Gao, Y., Zhang, J. & Zhao, F. Circular RNA identification based on multiple seed matching. *Brief Bioinform* **19**, 803-810, doi:10.1093/bib/bbx014 (2018).
42 Zhang, X. O. *et al.* Diverse alternative back-splicing and alternative splicing landscape of circular RNAs. *Genome Res* **26**, 1277-1287, doi:10.1101/gr.202895.115 (2016).
43 Gudas, L. J. & Wagner, J. A. Retinoids regulate stem cell differentiation. *J Cell Physiol* **226**, 322-330, doi:10.1002/jcp.22417 (2011).
44 Yamashita, T., Tucker, K. L. & Barde, Y. A. Neurotrophin binding to the p75 receptor modulates Rho activity and axonal outgrowth. *Neuron* **24**, 585-593, doi:10.1016/s0896-6273(00)81114-9 (1999).
45 Bothwell, M. Recent advances in understanding neurotrophin signaling. *F1000Res* **5**, doi:10.12688/f1000research.8434.1 (2016).
46 Ma, X., Zhou, Y., Chai, Y., Wang, X. & Huang, X. Stat3 Controls Maturation and Terminal Differentiation in Mouse Hippocampal Neurons. *J Mol Neurosci* **61**, 88-95, doi:10.1007/s12031-016-0820-x (2017).
47 Lyu, J. *et al.* The protein phosphatase activity of PTEN is essential for regulating neural stem cell differentiation. *Mol Brain* **8**, 26, doi:10.1186/s13041-015-0114-1 (2015).
48 Hyun, D. H. *et al.* The plasma membrane redox enzyme NQO1 sustains cellular energetics and protects human neuroblastoma cells against metabolic and proteotoxic stress. *Age (Dordr)* **34**, 359-370, doi:10.1007/s11357-011-9245-1 (2012).
49 Long, Y. *et al.* Conserved RNA-binding specificity of polycomb repressive complex 2 is achieved by dispersed amino acid patches in EZH2. *Elife* **6**, doi:10.7554/eLife.31558 (2017).

50 Long, Y., Wang, X., Youmans, D. T. & Cech, T. R. How do lncRNAs regulate transcription? *Sci Adv* **3**, eaao2110, doi:10.1126/sciadv.aao2110 (2017).
51 Hudson, W. H. & Ortlund, E. A. The structure, function and evolution of proteins that bind DNA and RNA. *Nat Rev Mol Cell Biol* **15**, 749-760, doi:10.1038/nrm3884 (2014).

Figure legends

Figure 1 - Determining the circRNA inventories of mESC, NPC and differentiated glutamatergic neurons and their differential regulation.
(A) Schematic illustration of work-flow for differentiation and RNA-seq. (**B)** Number of circRNAs detected by indicated circRNA prediction algorithm in different stages. (**C)** Venn-diagram showing 1449 common circRNAs of a total of 3581 circRNAs that are either constant or enriched upon RNase R treatment. (**D)** circRNA/circRNA+linear precursor ratios as a function of expression level (RPM) at the 3 sequenced stages. (**E)** Left: Heatmap showing differential expression of top-100 expressed circRNAs (RPM scale to the right), with selected examples of circRNAs as indicated along with genomic corrdinates. Top: K-means analysis displaying 5 different expression profiles during differentiation (same color code given to the left of the heatmap). (**F)** circRNA qRT-PCR strategy spanning the backsplicing junction. **(G)** qRT-PCR validaton of selected circRNAs. Data are depicted as mean ±SD.

Figure 2 - circZNF827 regulates neuronal marker expression levels.
(A) Knockdown of circZNF827 with dicer-independent short hairpin RNAs (dishRNAs) in the neuroblastoma cell line L-AN-5 increases mRNA expression levels of the neuronal markers TUBB3, MAP2, NEFL, and TrkB **(B)**. The mRNA expression levels were evaluated by RT-qPCR after four days of RA-mediated neuronal differentiation. **(C)** Increased expression of TUBB3 and MAP2 upon circZNF827 knockdown validated by western blotting (left panel). The results of quantification of band intensities from western blots are shown in middle and right panel. **(D)** Proliferation assay based on flow cytometric measurements of EdU incorporation into newly synthesized DNA shows increased replication rate upon circZNF827 knockdown. Data are depicted as mean ±SD. *$p<0.05$; **$p<0.01$; ns, not significant.

Figure 3 - Increased RAR expression upon circZNF827 knockdown.
(A) circZNF827 knockdown in L-AN-5 cells causes increased mRNA expression levels of RARα and RARγ. **(B)** Subcellular localization of the circRNAs circZNF827, circANKIB1, and circTULP4 examined after fractionation of differentiated L-AN-5 cells into cytoplasmic and nuclear fractions. GAPDH mRNA and β-actin pre-mRNA levels was used for validation of the purity of the cytoplasmic and nuclear fractions. **(C)** BrU pulse-chase mRNA decay assay evaluating decay rates of RAR mRNAs upon circZNF827 knockdown. The mRNA and circRNA expression levels were evaluated by RT-qPCR. Data are depicted as mean ±SD. *$p<0.05$; **$p<0.01$.

Figure 4 - circZNF827 regulates NGFR expression. (A) Nanostring analysis of the expression of ~800 neuropathology-related genes upon circZNF827 knockdown in L-AN-5 cells. **(B)** GO-term analysis based on genes found differentially expressed by the Nanostring analysis upon circZNF827

knockdown. **(C)** Validation of increased NGFR expression by western blotting upon circZNF827 knockdown. The result of quantification of band intensities from western blots is shown in the graph below the western blot. **(D)** BrU pulse-chase mRNA decay assay evaluating decay rates of NGFR mRNAs upon circZNF827 knockdown. **(E)** mRNA transcription rates estimated after BrU-labeling of newly synthesized RNA by Nanostring analysis using the neuropathology panel. **(F)** RT-qPCR-based validation of the Nanostring analysis showing increased NGFR mRNA transcription upon circZNF827 knockdown. **(G)** NGF stimulation of mediates enhanced NGFR signaling upon circZNF827 knockdown as shown by increased c-fos mRNA expression. Data are depicted in C as mean ±SEM and in D, F, and G as mean ±SD. **p<0.01.

Figure S1 – (A) Brightfield image of mESCs subjected to neuronal differention (neuron day 1, 3 and 8). (**B)** qRT-PCR on pluripotency and neuronal markers (Nanog, Nestin, TrkB and TUBB3) at different stages in differentiation. (**C)** Quantification of RNase R resistant circRNAs. Fraction of either depleted, unaffected or enriched of total number of circRNAs upon RNase R treatment as a result of using indicated circRNA prediction algorithm. (**D)** Expression levels of depleted, unaffected or enriched circRNAs (RPM). (**E)** circRNA-flanking introns are longer than average intron length of other host pre-mRNA introns. (**F)** Higher frequency of inclusion of 5'proximal exons in circRNAs.

Figure S2 - (A) Evaluation of dishRNA-mediated knockdown efficiencies of circZNF827 in mESCs, P19 cells and SHSY-5Y cells by RT-qPCR. **(B)** Evaluation of increased mRNA expression levels of the neuronal markers TUBB3, MAP2, NEFL, and TrkB upon RA-mediated neuronal differentiation of SHSY-5Y cells. The mRNA expression levels were evaluated by RT-qPCR. **(C)** Knockdown efficiencies of the circRNAs circSLC8A1, circHDGFRP3, circCDYL, circZNF609, circCAMSAP1, circUNC79, circANKIB1, and circTULP4 in L-AN-5 cells measured by RT-qPCR using circRNA-specific primers. **(D)** Expression levels of the neuronal markers TUBB3, MAP2, TrkB, and NEFL upon circRNA knockdown in L-AN-5 cells evaluated by RT-qPCR. **(E)** Validation of unaffected linear ZNF827 (linZNF827) mRNA levels upon knockdown of circZNF827 in L-AN-5 cells. Data are depicted as mean ±SD.

Figure S3 - (**A)** RAR mRNA transcription rates estimated after BrU-labeling of newly synthesized RNA. Data are depicted as mean ±SD. *p<0.05.

Figure S4 - (**A)** Increased NGFR mRNA expression upon circZNF827 knockdown in L-AN-5 cells validated by RT-qPCR. Data are depicted as mean ±SD.

Figure 1

A

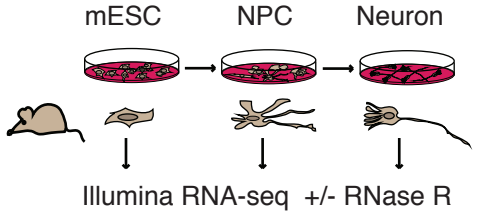

B

Pipeline/stage	mESC	NPC	Neuron
CIRCexplorer2	1167	2893	2177
CIRI2	792	2230	1902
find_circ	1150	2698	2316

reads backsplicing junction (circRNAs)

C

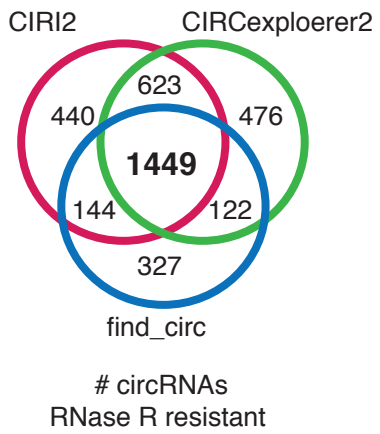

D

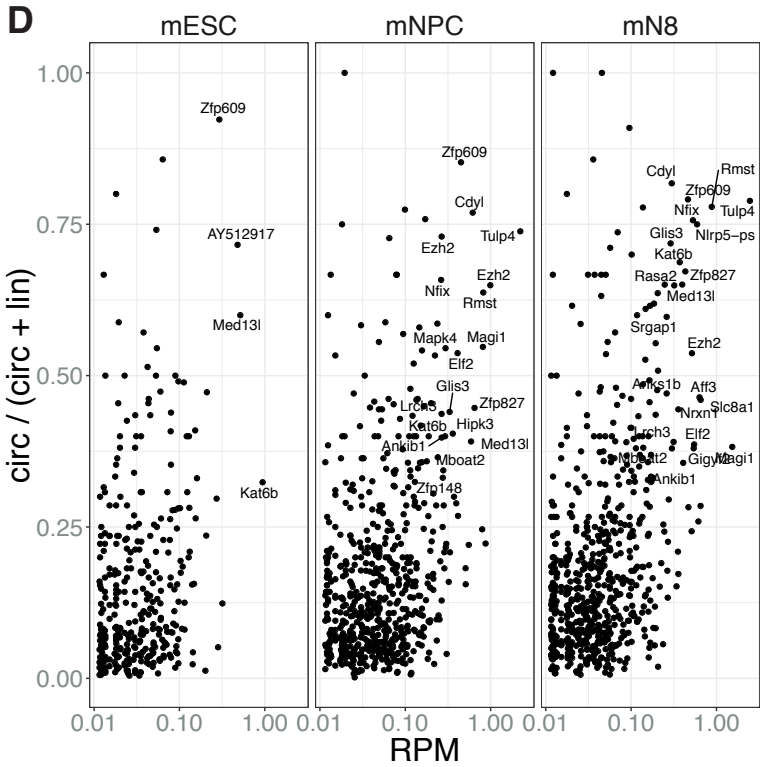

E

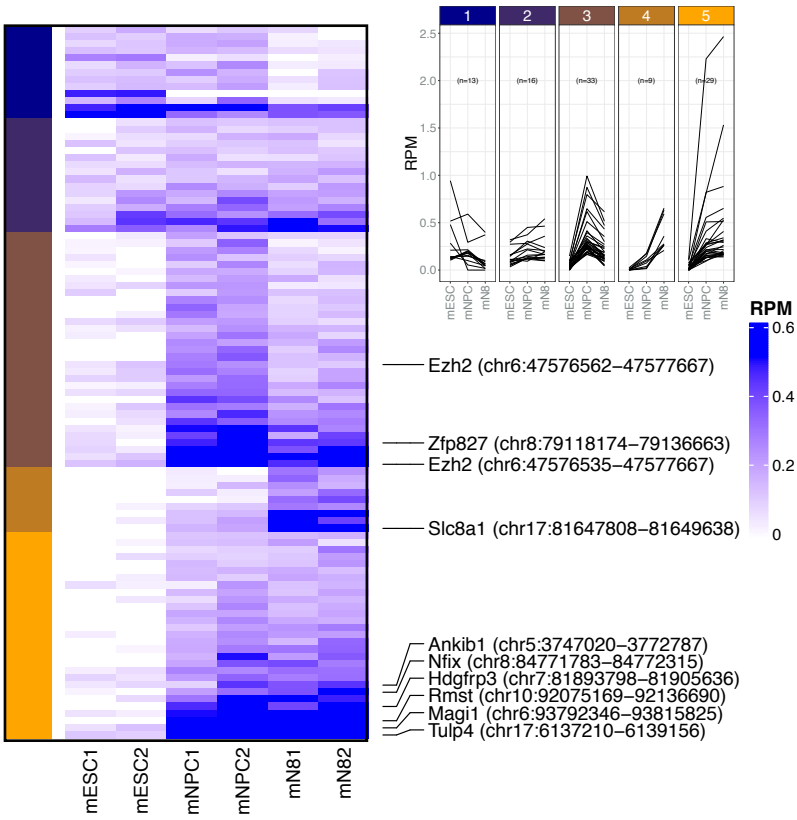

F

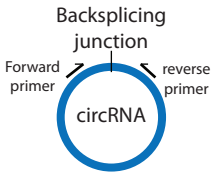

G

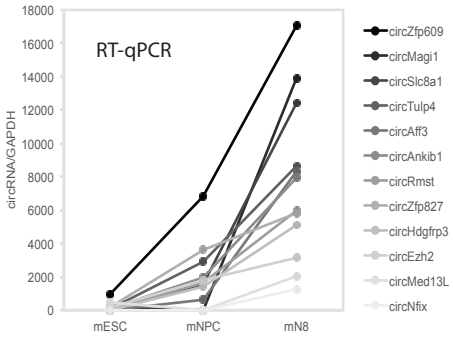

Figure 2

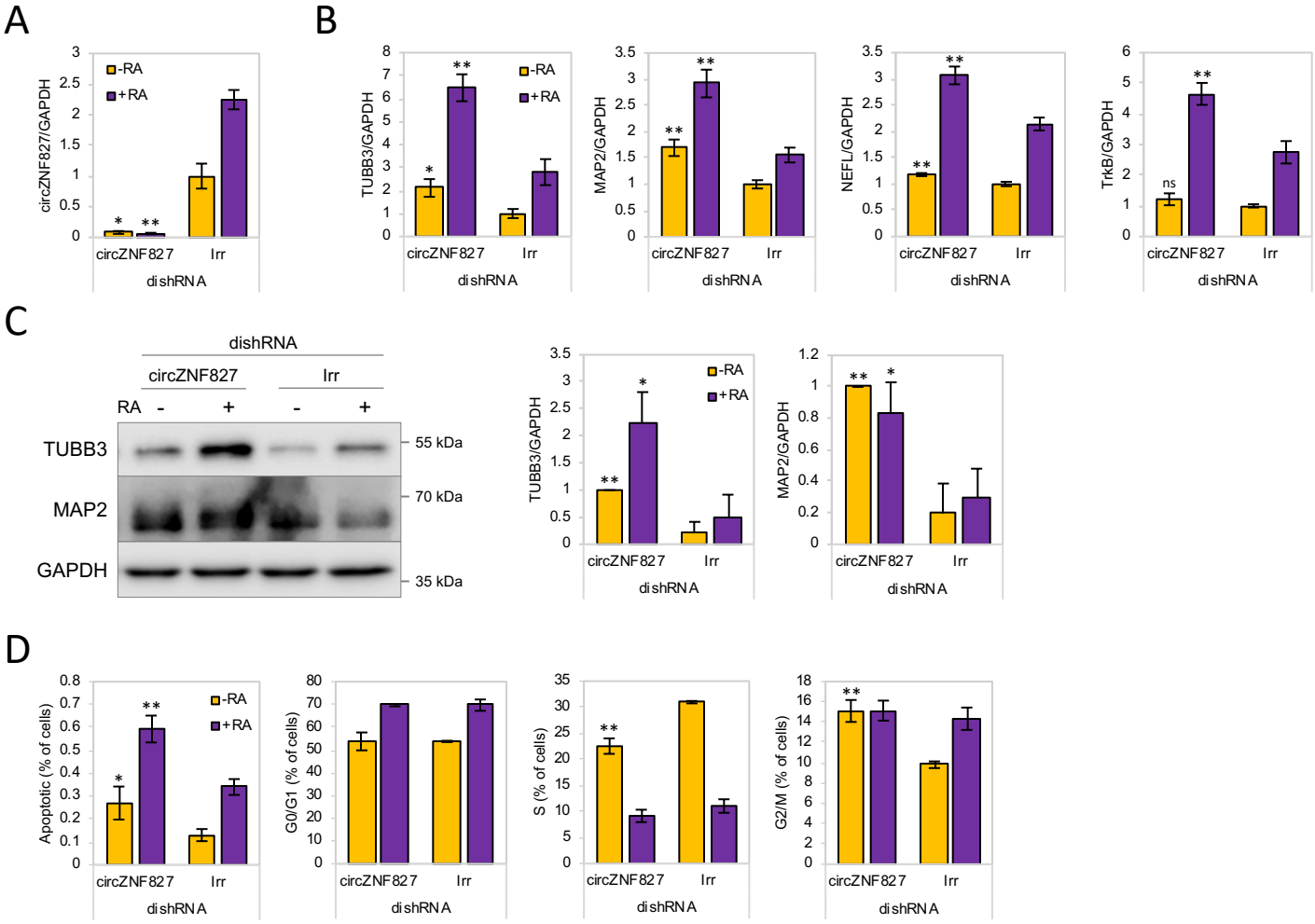
A
circZNF827/GAPDH
-RA
+RA
circZNF827
Irr
dishRNA
B
TUBB3/GAPDH
MAP2/GAPDH
NEFL/GAPDH
TrkB/GAPDH
ns
C
dishRNA
circZNF827
Irr
RA
TUBB3
MAP2
GAPDH
55 kDa
70 kDa
35 kDa
D
Apoptotic (% of cells)
G0/G1 (% of cells)
S (% of cells)
G2/M (% of cells)

Figure 3

A

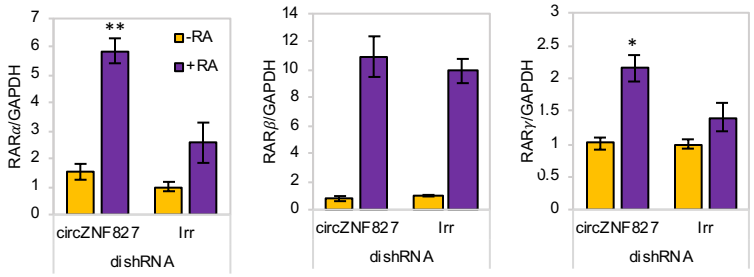

B

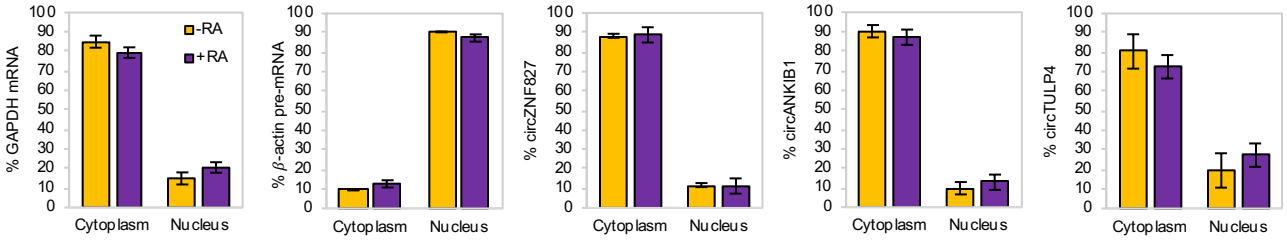

C

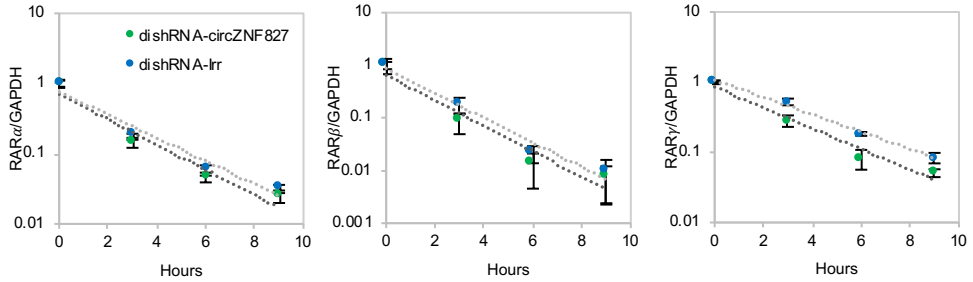

dishRNA	circZNF827	Irr
$T_{1/2}$ (hours)		
RARα	1.68 ±0.06	1.84 ±0.12
RARβ	1.22 ±0.20	1.28 ±0.34
RARγ	2.04* ±0.08	2.46 ±0.23

Figure 4

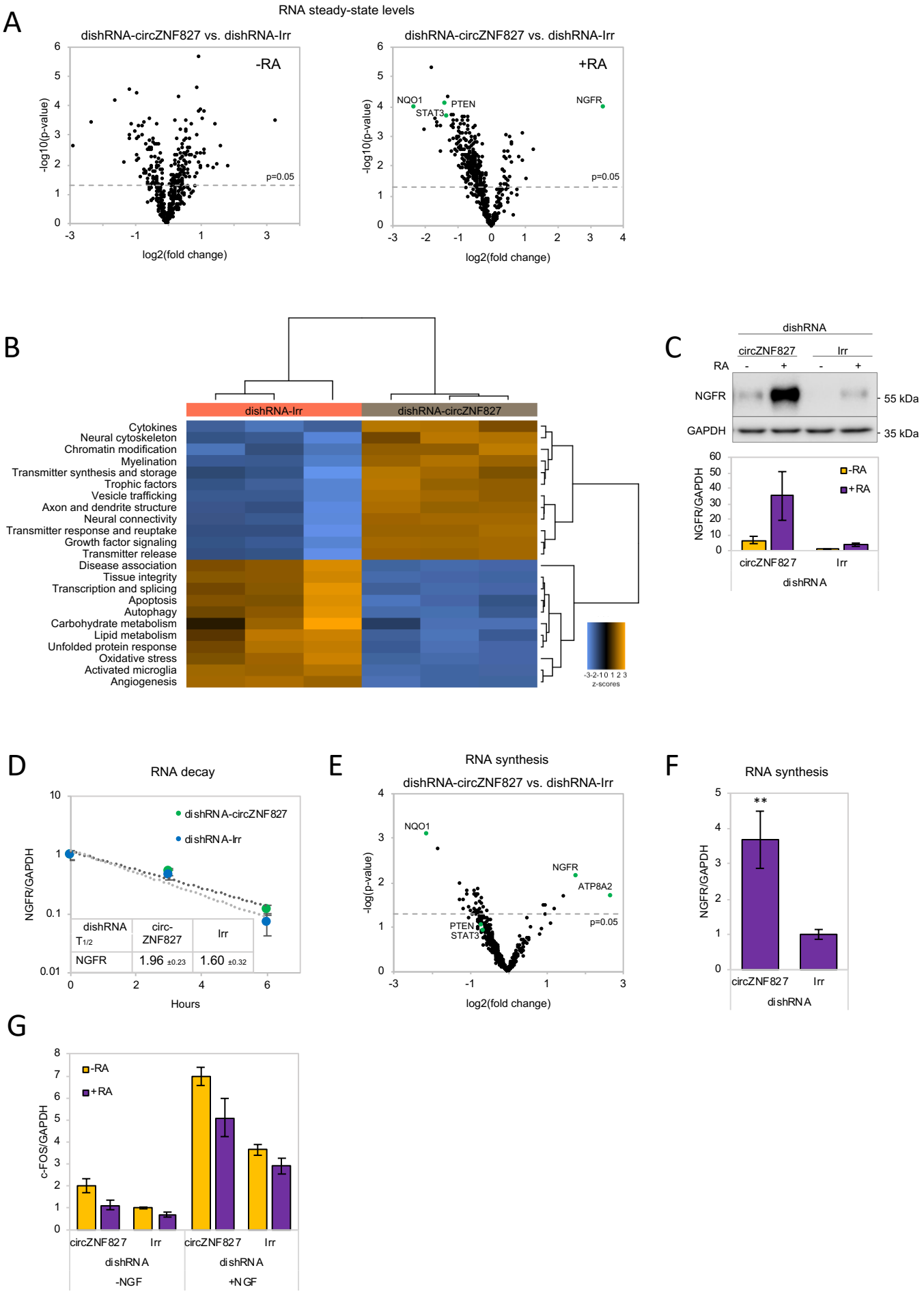
A
RNA steady-state levels
dishRNA-circZNF827 vs. dishRNA-Irr
-RA
+RA
-log10(p-value)
log2(fold change)
p=0.05
NQO1
STAT3
PTEN
NGFR
B
dishRNA-Irr
dishRNA-circZNF827
Cytokines
Neural cytoskeleton
Chromatin modification
Myelination
Transmitter synthesis and storage
Trophic factors
Vesicle trafficking
Axon and dendrite structure
Neural connectivity
Transmitter response and reuptake
Growth factor signaling
Transmitter release
Disease association
Tissue integrity
Transcription and splicing
Apoptosis
Autophagy
Carbohydrate metabolism
Lipid metabolism
Unfolded protein response
Oxidative stress
Activated microglia
Angiogenesis
z-scores
C
dishRNA
circZNF827
Irr
RA
NGFR
GAPDH
55 kDa
35 kDa
NGFR/GAPDH
-RA
+RA
circZNF827
Irr
dishRNA
D
RNA decay
dishRNA-circZNF827
dishRNA-Irr
NGFR/GAPDH
Hours
dishRNA T1/2
circ-ZNF827
Irr
NGFR
1.96 ±0.23
1.60 ±0.32
E
RNA synthesis
dishRNA-circZNF827 vs. dishRNA-Irr
-log(p-value)
log2(fold change)
NQO1
NGFR
ATP8A2
PTEN
STAT3
p=0.05
F
RNA synthesis
NGFR/GAPDH
circZNF827
Irr
dishRNA
G
-RA
+RA
c-FOS/GAPDH
circZNF827
Irr
dishRNA
-NGF
+NGF